 doi:10.20944/preprints202205.0233.v1

Article

Dynamic Texture Analysis of Water Flow Video Using Temporal Binary Pattern Image Histogram Neural Network

Bernadus Herdi Sirenden [1,2], Petrus Mursanto [1]* and Sensus Wijonarko [2]

[1] Faculty of Computer Science, Universitas Indonesia, Depok, Indonesia; santo@cs.ui.ac.id (P.M.); bernadus.herdi91@ui.ac.id (B.H.S)
[2] Indonesia National Research and Inovation Agency (BRIN), Puspiptek South Tangerang, Indonesia; sens001@@brin.go.id (S.W.); bern002@brin.go.id (B.H.S)
* Correspondence: santo@cs.ui.ac.id

Abstract: Water surface velocity is one of important parameter in hydrology. The development of non-intrusive measurement of this parameter using cameras is increasing. Traditionally the measurement of Water surface velocity using a camera utilizes tracking of moving objects that are exist on its surface. Recently, other methods have emerged that utilize the movement of water ripples to estimate these parameters. This paper proposes a novel method for estimating Water surface velocity based on cameras measurement. We name this method Temporal Binary Pattern (TBP), since it extract binary pattern of pixels of water flow video in time domain using XOR operator. The pattern formed from the extraction is then used to create a new image which we call a Temporal Binary Pattern Image (TBPI). Then the histogram of the new image is used as input for the Feed-forward Neural Network which will correlate it with the water velocity. Since it use Neural Network the final name of the proposed method is Temporal Binary Pattern Image Histogram Neural Network (TBPIHNN). We develop Mini Open Channel Water Flow Simulator (MOCWFS) to provide video data set for TBPIHNN. After training the accuracy achieved is 73%. We tested the method in 4 different pump speeds, at 2 low pump speeds the TBPI formed was significantly differentiated. But not so at the other 2 higher speeds.This is due to the resolution of TBPI on each pixel which is only 8 bits, and also the reason why TBPIHNN training accuracy can only reach a maximum of 73%.

Keywords: water surface velocity; image based measurement; dynamic texture analysis

1. Introduction

Water Surface Velocity (WSV) estimation is one of important parameter in environmental monitoring. It is useful to perform empirical calibration of rating curve [1]. This curve combine with remote sensing data of river stage can be use to estimate river discharge. The most respectfull method to estimate WFV is by using Acoustic Doppler Current Profiler (ADCP) [2,3]. But this methods are quite dangerous since for some river where there are no bridge present, human operator need to be near the water to perform measurement[1]. Other than safety reasons, above method also have poor spacial coverage [4]. Alternatively measurement of WSV using non-intrusive method had been investigated. Some non-intrusive method use radars [5], and some use camera[1,3,4,6–23]. Radars technology were more expensive, time consuming, and require qualified personnel, while camera or optic base method were inexpensive, and flexible installation either in fixed permanent location or mounted in UAV [19]. Although WSV are not the same as depth-averaged velocity (DAV),which is needed to estimate discharge[2], Genç et.al [9] work show that there are linear relationship between WSV and DAV. They use camera based method to measure WSV, the error between WSV and DAV are about 4.08%.

The common method to estimate WSV using camera are Particle Tracking Velocimetry (PTV)[4,7] and Particle Image Velocimetry (PIV)[1,6,7,17,21]. Both of these method and their variants utilize moving particle to estimate WSV. The difference betwen those two

 doi:10.20944/preprints202205.0233.v1

are number of tracking particles. PTV track single particle or object in river surface, while PIV track group of particles[4,17]. Beside using PIV or PTV, which use correlation-based algorithms, there are other method which estimate WSV using moving particle or object, such as Optical Flow (OF) based algorithms [8,19]. Elter et. al. [7] also use PIV and PTV to estimate WSV from thermal signature of river flow, which replace the need of particle. Thermal signature are captured using Thermal camera for PIV, and RGB Camera for PTV.

There are also exist other types of methods which do not utilize moving particle or object to estimate WSV. Many of them utilize dynamic movement of water ripple to estimate WSV. Among them are Space Time Image Velocimetry (STIV) created by Fujita et.al in 2007 [10], Farneback Optical Flow Method (FOFM) by Wu et.al in 2019[8], and Galois-Field Representation by Sirenden et.al in 2020 [23]. The first three are originate from the same root, which is Optical Flow (OF) method . General mathematical formulation of OFM is first proposed by Horn-Schunk in 1981 [24]. The basic hypothesis of OF are gray level invariant hypothesis, which is stated that the gray level observed at any object point remains unchanged for a short time. So when there is a change in the gray level of pixels it is most likely caused by physical motion. In OF method direction are required since it calculate two velocity vector in x and y direction of the image frame[3,8,19,24]. So to able to capture WSV the velocity vector of water flow should be parallel with one of OF velocity vector.

The last of the four method mentioned in previous paragraph, are base upon histogram similarity of dynamic texture of water flow video. The hypothesis of GFR method are water flow video texture exhibit periodic pattern. This periodic pattern is captured by examining the Euclidean Distance (ED) of histogram using auto-correlation function. The original image frame of video were transformed to GFR so its independent of water flow direction. The original frame of the video is transformed to GFR so that it does not depend on the direction of the water flow. Unlike the OF-based method where the application of OF is aligned with the direction of the water flow.

In image texture analysis each pixels are compared with its surrounding neighbours. For static image, pixel comparison were performed in spatial domain. For dynamic image sequences analysis, such as videos, pixel comparison were conducted in spatial and temporal domain. One of advantage of pixels comparison method is do not required mathematical operation such as partial derivative as we can see in all OF based method. For example in Local Binary Pattern (LBP) and its variants [25–29], Local Binary Count (LBC) and its variants [27], the calculation is base upon logical operation. Other type of static texture analysis use bit-wise operation such as XOR which is computationally lighter [30,31].

In this paper We introduce new dynamic texture descriptor namely Temporal Binary Pattern (TBP), which use XOR operator to extract temporal feature of dynamic texture of video image. We combine Histogram of Image formed by TBP and Feed-forward Neural Network to form TBPIHNN. We train TBPIHNN with water surface flow video produced by Mini Open Channel Water Flow Simulator (MOCWFS) to estimate changes of volume flow rate. This changes of volume flow rate are proportional to WSV.

2. Related Work

2.1. Space Time Image Velocimetry

STIV analyze water ripple motion to estimate WSV. To do this STIV draws imaginary lines in the direction of the water flow.The brightness variation of the pixels in these lines are use to construct a space-time frame called a Space-Time Image (STI). The gradient of gray level intensity in each local windows which construct STI then calculated. Then the orientation of each local windows also calculated. As a final step, mean of orientation angle from the orientation angles obtained for the local windows is calculated. This mean orientation angle is proportional to WSV [10–12,14,15,22]. Due to its high spatial resolution and low time complexity STIV is potential method for real time application [22]. STIV had

 doi:10.20944/preprints202205.0233.v1

been compared with other method such as PIV [10], ADCP [11], propeler flowmeter [16], and agree fairly.

Despite its advantages, STIV is still being improved by several researchers. The quality of STI can be affected by noise in real time aplication, for example measurement of WSV during bad weather or nigth time or other factor which exist in nature [12,15,22]. Fujita et.al [12], proposed new algorithm using auto-corelation function for STI which is differ to original STI which use 2-D Fourier Transform. This new algorithm are called QESTA. Zhao et.al [22] proposed new denoising method and combined with Fast Fourier Transform (FFT) based STIV to improve accuracy due to low quality of STI. Watanabe et.al [15] use Convolution Neural Network (CNN) to overcome low quality STI. CNN are use to automatically detect STI gradient pattern. The input to CNN are 2-dimensional Fourier Transform Image of STI (2DFTISTI). Identification of pattern gradient by CNN are more easy to do by in 2DFTISTI compared to original STI.

While the above methods concentrate on accuracy and robustness of STIV, the following researcher try to modify STIV to develop new method which independent to direction of imaginary search line. Tsuji et.al [14] develop a method called Space Time Volume Velocimetry (STVV), which based on STIV. It try to overcome the need to generate imaginary lines parallel to water flow direction. Instead of generate STI, this method generate Space Time Volume (STV) and analyzed using 3-dimensional Inverse Fourier Transform. Han et.al [16] proposed two dimensional STIV, where the search line were rotated to find the STI which has the most prominent oblique stripes. They develop the method to overcome the shortcoming of STIV due to the requirement of predetermined search angle, and STVV accuracy which depend heavily on the angle recognition error due to difficulty to recognition of space angle compared to plain angle.

2.2. Farnelback Optical Velocimetry

Wu et.al [8] use Farneback Optical Flow Method (FOFM) to estimate WSV. By comparing FOFM with physical measurement by a portable propeller velocimeter in standard trapezoidal open channel flow testbench, it is found that FOFM and portable propeller agree with in 4.5%, and it is required 150 frame of images to have stable WSV measurement result. Similar with STIV, FOFM need to identify the direction of water flow first. FOFM are considered Dense Optical Flow (DOF) type of OFM [8], while STIV is Tensor Based (TB) type [10,24]. Previously Paygude et.al [32] had combine FOFM with Gabor Filter to detect velocity and orientation of traffic and cloud movement in real time application. FOFM is use to estimate velocity, while Gabor Filter is use to detect orientation.

2.3. Galois Field Representation

WSV estimation using a camera is basically a dynamic texture analysis problem. As seen in STIV the dynamic texture analysis is carried out in space and time framework. Dynamic texture can be considered a changes or variant in gray level of pixels value as we can see in STIV and FOFM method. The author had also proposed method to analyse WSV from video based on idea that water flow video exhibit periodic pattern. To capture this periodic pattern the author use spatial and temporal feature extraction separately. First the static image in each frame were transform to other representation using Galois Field addition operator, which is XOR. This new representation are called Galois Field Representation (GFR). Then two spatial feature, Histogram and Normalized Cumulative Histogram (NCH), will be extracted from GFR. To extract temporal feature, Euclidean Distance (ED) applied to measure similarity between spatial feature of the first frame and the rest of the frame. The ED metric then will be analyze using auto-correlation function to determine the periodicity of dynamic texture of water flow video. The periodicity of ED is assumed to be proportional to the WSV. The result of experiment shows that NCH is perform better as spatial feature compared to Histogram [23]. The idea of using Galois Field is inspired by Shivashankar et al. [30,31], which apply GFR to static texture classification such as face recognition and other texture, which invariant to rotation and scale changes.

Preprints (www.preprints.org) | NOT PEER-REVIEWED | Posted: 17 May 2022 doi:10.20944/preprints202205.0233.v1

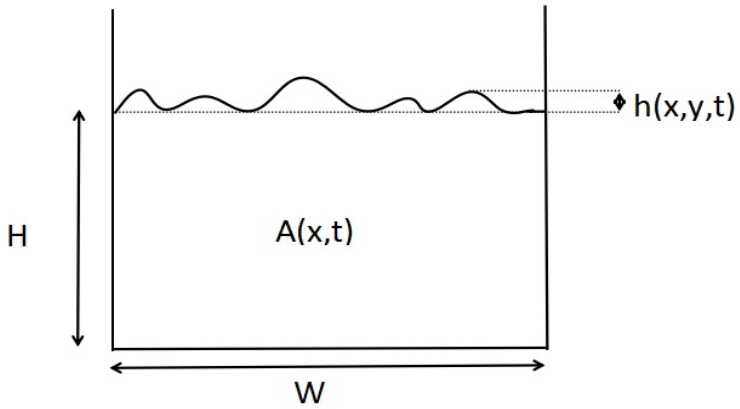

Figure 1. Visualization of SWE in front view of OCC

In GFR method each of pixel were transformed into new representation by mean of XOR operation of central pixel with 8 local neighbouring pixels.

2.4. Local Binary Pattern and its variants

Similar strategy also exist in Local Binary Pattern (LBP) method, where the central pixel become threshold value for other 8 local neighbouring pixels. When the value of one pixel in neighbouring pixels are lower or same with central pixel, than the value of that pixel location become 0, otherwise the value become 1. Since the new transformation value only 0 and 1, the method is named LBP [25–29]. Other method which developed from LBP is Local Binary Count (LBC), the difference is in how the result are being presented. In LBP the result is being presented as byte for example 11111111 is 256, while in LBC the result is count of how many 1, so in the example it is 9 for LBC. The motivation of LBC development is to reduce the size of final result[27].

With the reason popularity of Machine Learning, some researcher combine LBP and their variants with Neural Network (NN).Xu et.al [26] reformulate traditional method of encoding in LBP to convolutional filters which is use in CNN. This reformulation lead to design of Local Binary Convolution Neural Network (LBCNN). They compared LBCNN with other NN algorithm using MNIST, SVHN, CIFAR-10, ImageNet, and demonstrates excellent performance and perform as well as standard CNN. Wei et.al [29] combine CNN and LBP to classify hyperspectral image with very high spectral resolution. They use two-dimensional CNN (2D-CNNN), the first one dimensional CNN (1D-CNN) extract hierarchical spectral features and another same 1D-CNN is applied to process LBP features to further extract spatial features. The demonstration of this method show that it can provide good classification accuracy on limited training samples.

For dynamic texture analysis or classification, evolve to Volume LBP (VLBP) and LBP from Three Orthogonal Planes (LBP-TOP). Both of these method use 3D-spaces which is X, Y (2D spatial frame) and T (time frame) axis. In VLBP the operation of LBP were conducted in 3D surrounding pixels of centre pixel. The number of patterns in VLBP is will increase by 2^{3P+2}, where P is the number of surrounding pixels, so the number will be very large. Due to this, Ma and Cisar [25] proposed LBP-TOP. In LBP-TOP, LBP were carried out in three separated 2D planes, which is XY, XT and YT. After LBP operation is performed, the histogram of this three orthogonal planes then joined. By using this strategy the number of bin or patterns is reduced to $3 \cdot 2^P$. Zhao et.al [27] develop Volume LBC (VLBC) which combine LBC and VLBP. This method able to include more neighboring pixels without exponentially increasing the feature dimension as VLBP does, and run much faster than VLBP and LBP-TOP.

Preprints (www.preprints.org) | NOT PEER-REVIEWED | Posted: 17 May 2022 doi:10.20944/preprints202205.0233.v1

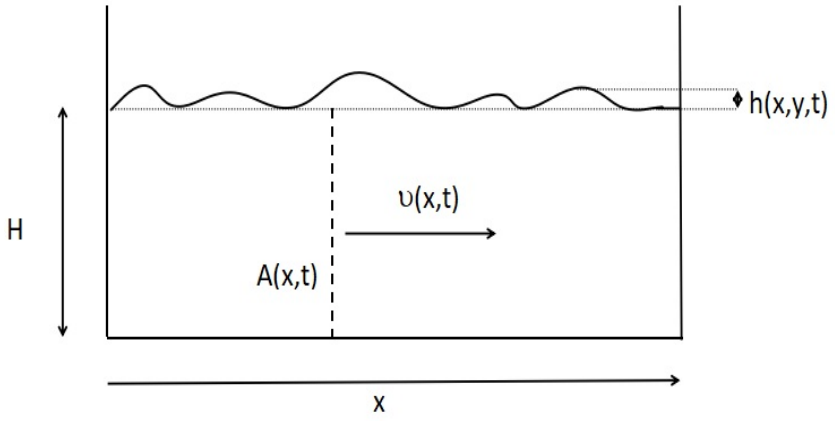

Figure 2. Visualization of SWE in side view of OCC

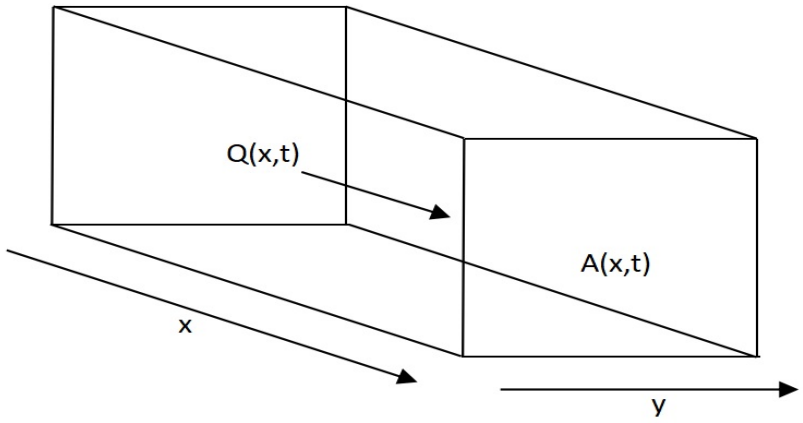

Figure 3. Visualization of Saint Venant Equation in OCC

3. Proposed Method

Consider three dimension physical boundary of open channel where water is flowing through as shown in Fig. 3, where $Q(x,t)$ is water discharge and $A(x,t)$ is cross-sectional area of water flow, which vary over x direction and time t. Hereafter we call this physical boundary as Open Channel Column (OCC). For shallow water that flowing inside OCC, famous equation called Saint Vennant capture fluid motion behaviour as is shown in equation 1. This formula also called Shallow Water Equation (SWE) and its derived from Navier Stokes equation [33].

$$\frac{\partial A(x,t)}{\partial t} + \frac{\partial Q(x,t)}{\partial x} = 0 \tag{1}$$

If we take front view of OCC as shown in Fig. 1, we can derive $A(x,t)$ from the mean height of water in OCC (H), OCC width (W), water ripple height ($h(x,y,t)$), which is vary over x, y direction and time t. Mathematical formulation of this visualization is shown in equation 2. If we take side view of OCC as shown in Fig. 2, it can visualize that $Q(x,t)$ is a product of $A(x,t)$ and mean velocity ($v(x,t)$) as in equation 3.

$$A(x,t) = (H \cdot W) + \int (H + h(x,y,t))\mathrm{d}y \tag{2}$$

$$Q(x,t) = A(x,t) \cdot v(x,t) \tag{3}$$

Preprints (www.preprints.org) | NOT PEER-REVIEWED | Posted: 17 May 2022 doi:10.20944/preprints202205.0233.v1

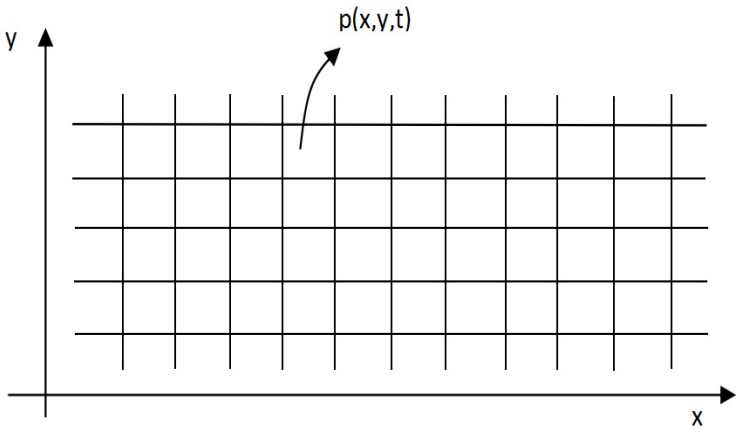

Figure 4. Visualization of Image Frame from Top View

As we can see in equation 1, it is necessary to have partial derivative of $A(x,t)$ over t and $Q(x,t)$ over x. The partial derivative of $Q(x,t)$ over x is given in equation 4, and we can see in that equation it is required to take partial derivative of $A(x,t)$ over x as well. Equation 5 and 6 show partial derivative of $A(x,t)$ over t and x. As we can see the from that equations that derivative of $A(x,t)$ over t and x are integral of partial derivative of $h(x,y,t)$ over t and x trough y direction.

$$\frac{\partial Q(x,t)}{\partial x} = A(x,t) \cdot \frac{\partial v(x,t)}{\partial x} + v(x,t) \cdot \frac{\partial A(x,t)}{\partial x} \tag{4}$$

$$\frac{\partial A(x,t)}{\partial t} = \int \frac{\partial h(x,y,t))}{\partial t} \cdot \mathrm{d}y \tag{5}$$

$$\frac{\partial A(x,t)}{\partial x} = \int \frac{\partial h(x,y,t))}{\partial x} \cdot \mathrm{d}y \tag{6}$$

Visualization of image frame taken by camera from top of OCC is shown in Fig. 4. The grid is representation of pixel ($p(x,y,t)$) which is vary over x , y and t. In water flow video this pixels change are related with water ripple change over x , y and t. So we can assume that partial derivative of $h(x,y,t)$ over x and t approximately represented by partial derivative of $p(x,y,t)$ over those axis. Equation 7 and 8 show this assumption in mathematical form.

$$\frac{\partial h(x,y,t)}{\partial t} \approx \frac{\partial p(x,y,t))}{\partial t} \tag{7}$$

$$\frac{\partial h(x,y,t)}{\partial x} \approx \frac{\partial p(x,y,t))}{\partial x} \tag{8}$$

In this paper the author consider to extract feature from change over time of each pixel in the video frame then transform it. Then take histogram of the transformation and use it as a learning parameter for FNN.

Preprints (www.preprints.org) | NOT PEER-REVIEWED | Posted: 17 May 2022 doi:10.20944/preprints202205.0233.v1

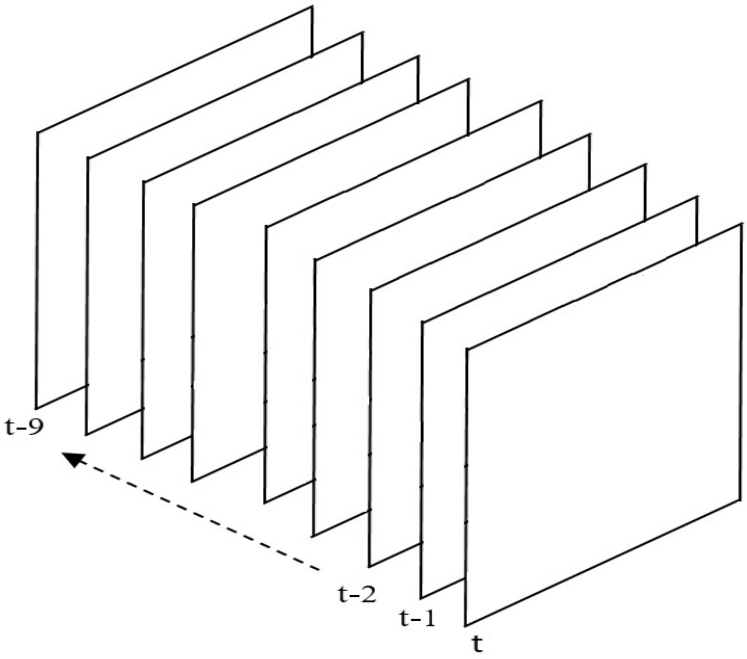

Figure 5. Frame Collection from t to $t-9$

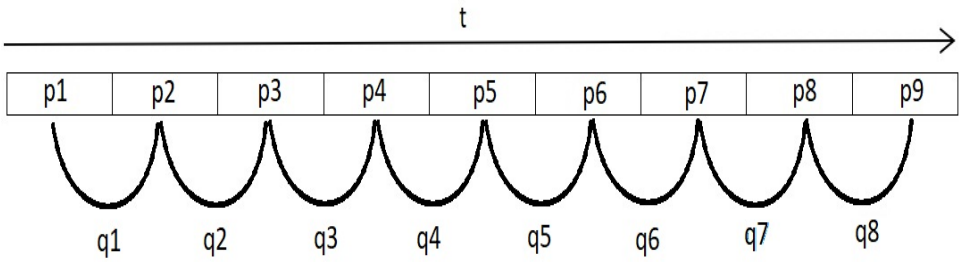

Figure 6. Temporal Binary Patern

3.1. Temporal Binary Pattern Image

To construct TBPI, we collect 9 frame. The first frame is at current time (t) and the last frame is at $t-9$ as shown in Fig. 5. In each pixel coordinate we collect 9 pixels in time direction as shown visually in Fig. 6 and mathematically in equation 9. We call this pixels collection as $p_n(x,y)$, where n is pixel index as shown in equation 10. In this paper we use gray-scale image. Pixels in a grayscale image have a range from 0 to 255. This number is in digital number format. This number range is a byte consisting of 8 bits. The bits $b_{m,n}(x,y)$ that make up the $p_n(x,y)$ are shown in the equation 11.

$$\begin{aligned} p_n(x,y) &= \{0,1,2,...,255\} \\ &= b_{1,n}b_{2,n}b_{3,n}b_{4,n}b_{5,n}b_{6,n}b_{7,n}b_{8,n} \end{aligned} \tag{9}$$

$$n = \{t, t-1, t-2, ..., t-9\} \tag{10}$$

$$b_{m,n}(x,y) = \{0,1\} \tag{11}$$

After that we construct $q_n(x,y)$ resulting from the XOR operation between p_n and p_{n-1} as shown in figure 6 and equations 12 and 13. Since it is an XOR operation, $q_n(x,y)$

Preprints (www.preprints.org) | NOT PEER-REVIEWED | Posted: 17 May 2022 doi:10.20944/preprints202205.0233.v1

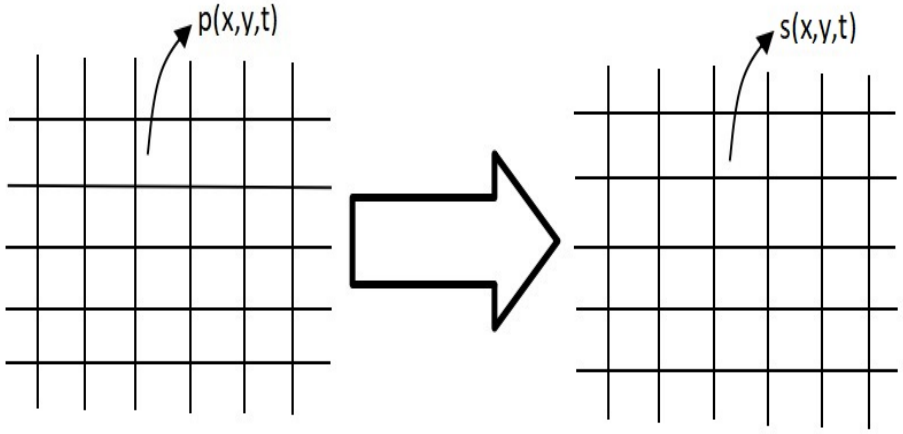

Figure 7. Transformation from original image frame ($p(x,y,t)$) to TBPI ($s(x,y,t)$)

will be the same size as $p_n(x,y)$. It also contains a collection of bits called $B_{m,n}(x,y)$. If we perform XOR operation for each $B_{m,n}(x,y)$ as shown in equation 14, we can have new variable called $r_n(x,y)$ which is one bit value. We collect this bit value and construct a new image called TBPI ($s(x,y,t)$) as shown in equation 15. TBPI may be vary in space and time (x,y,t), and have the same size with original image ($p_n(x,y)$). This transformation from $p(x,y,t)$ to $s(x,y,t)$ can be visualize in Fig. 7.

$$\begin{aligned} q_n(x,y) &= p_n(x,y) \oplus p_{n-1}(x,y) \\ &= B_{1,n}B_{2,n}B_{3,n}B_{4,n}B_{5,n}B_{6,n}B_{7,n}B_{8,n} \end{aligned} \tag{12}$$

$$B_{m,n}(x,y) = b_{m,n}(x,y) \oplus b_{m,n-1}(x,y) \tag{13}$$

$$r_n(x,y) = B_{1,n} \oplus B_{2,n} \oplus B_{3,n} \oplus B_{4,n} \oplus B_{5,n} \oplus B_{6,n} \oplus B_{7,n} \oplus B_{8,n} \tag{14}$$

$$s(x,y,t) = r_1r_2r_3r_4r_5r_6r_7r_8 \tag{15}$$

3.2. Temporal Binary Pattern Image Histogram

The transformation result $s(x,y,t)$ is also a image with the same size as $p(x,y,t)$. Since TBP had extract temporal dynamic feature, but not the spatial feature, we will use histogram as spatial feature extraction. The reason why histogram are chosen because it is independent on spatial orientation. This will be an advantage, because the proposed method will not be affected by the direction of the water flow. In this paper we use 11 bins to construct our histograms.

3.3. Feature Learning Using Feedforward Neural Network

The histogram of $s(x,y,t)$ which discussed before will become input for FNN. The structure of FNN is 11 input node, 2 hidden layer and 1 output layer. The output is numeric value, so our FNN is solving regression problem. Table 1 show the structure of FNN. We train the network using ADAM optimizer and Mean Absolute Error (MAE) as a loss function, 1000 epochs will be use in the training.

Preprints (www.preprints.org) | NOT PEER-REVIEWED | Posted: 17 May 2022 doi:10.20944/preprints202205.0233.v1

Network Structure		
Layer	Node	Activation
Input	11	ReLU
1^{st} Hidden	11	ReLU
2^{nd} Hidden	10	ReLU
Output	1	Linear

Training Parameter	
Optimizer	ADAM
Loss Function	MAE
Epochs	1000

Table 1. FNN Structure and Training Parameter

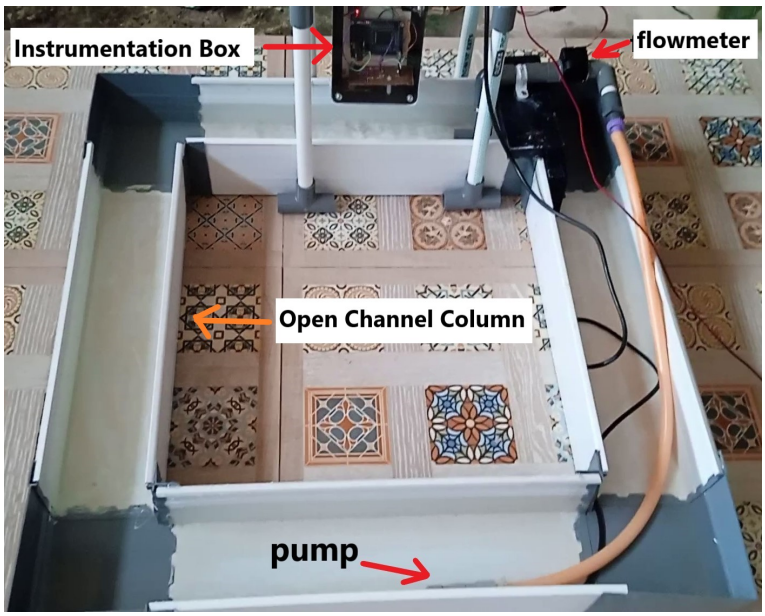

Figure 8. Mini Open Channel Water Flow Simulator

4. Experimental Setup

Water flow video data are collected from MOCWFS, which consist of Open Channel Column (OCC) made from PVC, small submersible pump, mini flow-meter and instrumentation box (IB). Figure 8 show the whole part of MOCWFS. OCC serves as a container of water, it's mechanical dimension are shown in Figure 9. Water are fill into OCC approximately 7 cm from bottom as shown in Figure 10. Camera sensor which is use to capture water surface are OV2460, which is integrated with ESP32 in ESP32-CAM module. As shown in Figure 11 ESP32-Cam are located in the bottom of IB, The distance of IB to the bottom of OCC is approximately 15.5 cm, therefore the distance of water surface to camera is about 8.5 cm as shown in Figure 12.

The water in the OCC is driven by a mini sumersible pump. The pump speed is controlled by the Field Programmable Gate Array (FPGA) inside the IB. Meanwhile, the volumetric flow rate of water produced by the pump is measured by a mini flow-meter. The flow-meter pulse data is sent to the FPGA. The FPGA and ESP32-Cam communicate with each other using a serial communication protocol. The ESP32-Cam transmits the pump's Pulse Width Modulation (PWM) data to FPGA, and receives flow-meter frequency data from it. The PWM data correlates with the pump speed, while the flow-meter frequency

Preprints (www.preprints.org) | NOT PEER-REVIEWED | Posted: 17 May 2022 doi:10.20944/preprints202205.0233.v1

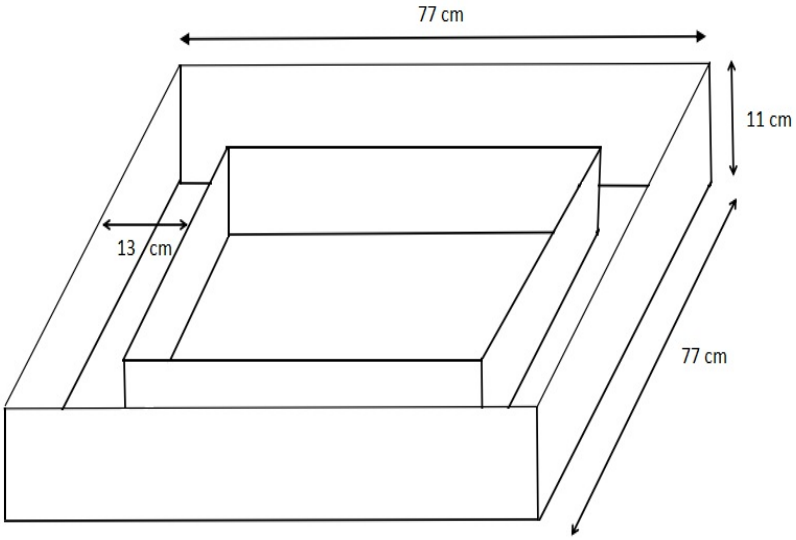

Figure 9. Open Channel Column Mechanical Dimension

Figure 10. Water Level inside OCC

data correlates with the volumetric flow rate as measured by the flow-meter. The flow-meter data received by the ESP32-Cam is forwarded to the PC when requested, the PC also sends the pump speed data to the ESP32-Cam. In addition to functioning as a wireless data trans-receiver, the ESP32-Cam also captures images of surface water flows and sends them to a PC.In the PC there is a Python program that functions to send pump speed data and receive surface water flow image data. The program utilizes the TCP-IP protocol to communicate with the ESP32-Cam continuously. Meanwhile, to receive the flow-meter data, the Hercules program is used, the user sends a certain command that tells the ESP32-Cam to send the flow-meter data. This data transaction does not occur continuously for fear of disturbing image data transactions. The communication protocol used for data flow-meter transactions is UDP. The processes described previously can be seen visually in Figure 13.

Table 2 show the pump specification. PWM data format which send by ESP32-Cam to FPGA is MxxxxxS. Where xxxxx is integer value from 0 to 9999, which corelated with PWM

Preprints (www.preprints.org) | NOT PEER-REVIEWED | Posted: 17 May 2022 doi:10.20944/preprints202205.0233.v1

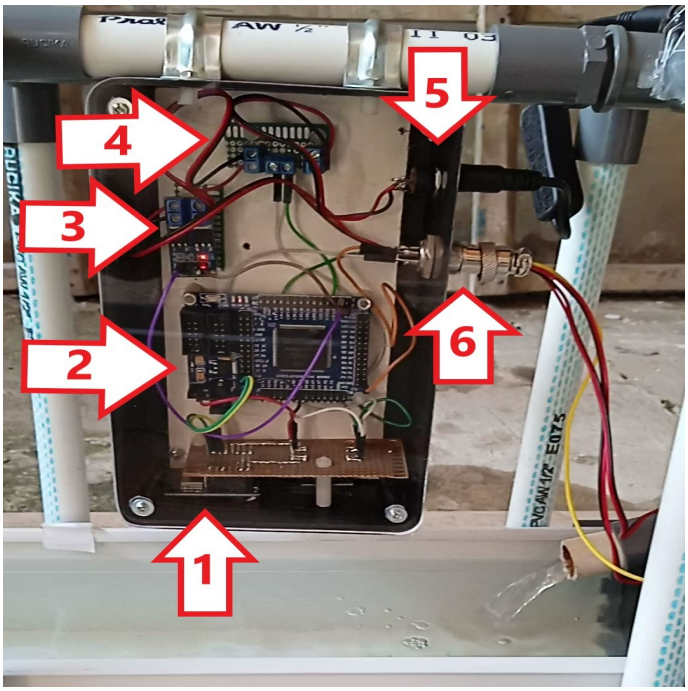

Figure 11. Instrumentation Box: 1) Esp32-Cam 2) FPGA 3) MOSFET 4) Connecting Circuit 5) Power Supply Connector 6) Connector to Flow-Meter and Pump.

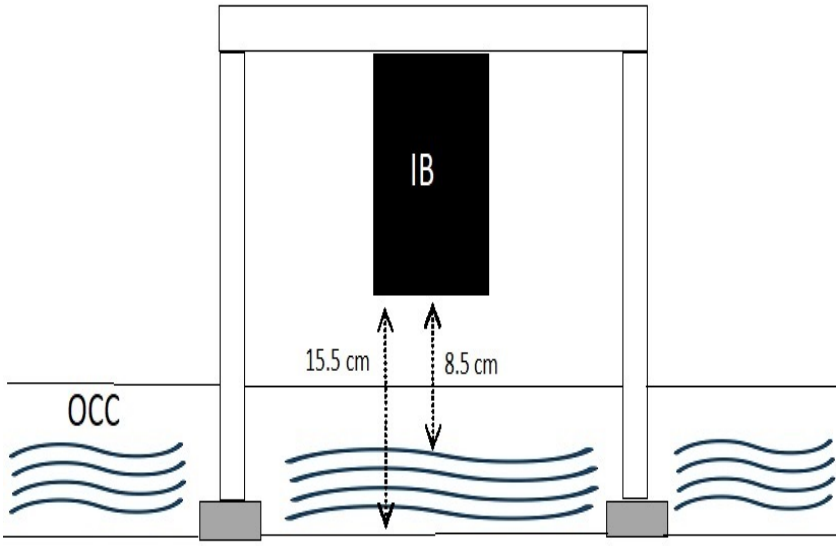

Figure 12. Distance of camera sensor to water level.

value. The author write VHDL code which create PWM generator which have period of 50 millisecond and resolution of 16 bit.

The specification of flow-meter can be seen in table 3. Data format send by FPGA to ESP32-Cam is BxxxxV, where xxxx is frequency value in range of 0 to 9999 Hz. K-Factor in that table is use to convert frequency data to volume flow rate. Frequency meter are created using VHDL inside FPGA, it has 1 Hz sampling rate.

The author use Cyclone II EP2C5T144 module. It is a low cost FPGA Development Board from Altera-Intel. It has 50 Mega Hz oscillator, maximum clock frequency is 300 MHz, JTAG programming connector, EPCS4SI8 4 Mega byte serial configuration flash, active Serial connector for programming, 5 Volt power jack, , 89 I/Os, 3.3 Volt (I/O) and 1.2

Preprints (www.preprints.org) | NOT PEER-REVIEWED | Posted: 17 May 2022 doi:10.20944/preprints202205.0233.v1

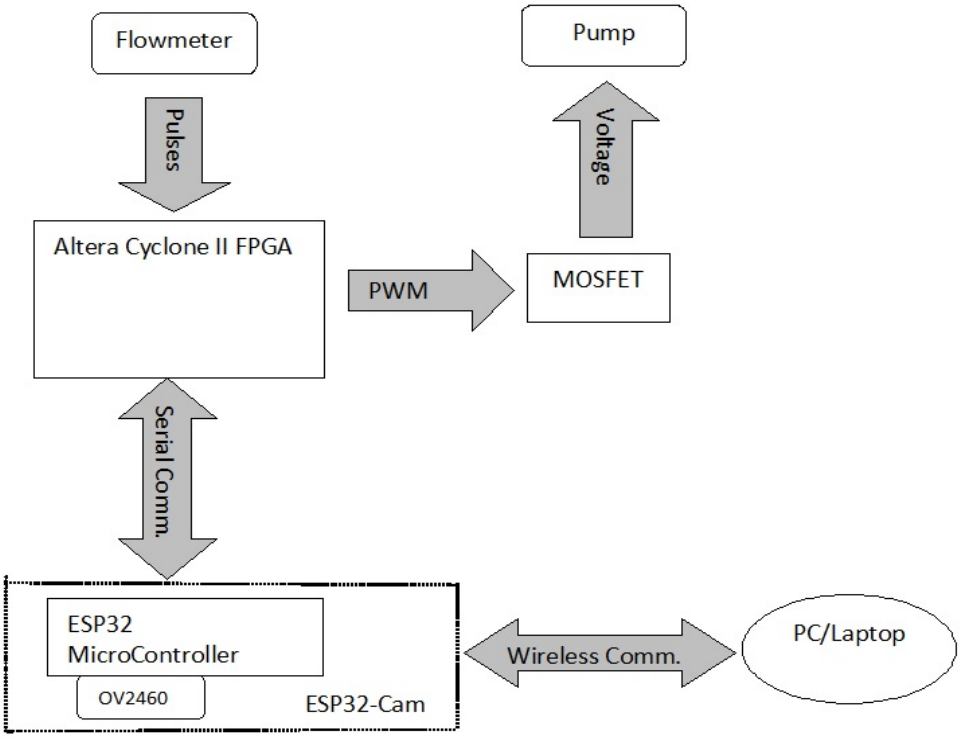

Figure 13. Sigral Trancsaction Between Electronic Component inside IB and PC/Laptop.

Characteristic	Value
Maximum Flow	14 Litre/Minute
Working Voltage	12 VDC
Maximum Current	1.2 A
Maximum Suction	5 metre
Pump Type	Submersible

Table 2. Characteristic of Mini Submersible Pump

Characteristic	Value
Model	YF-S201
Flow Range	1-30 Litre/Minute
Voltage Range	3.5-24 VDC
Connection Cable	Three Wire (Power, Signal, Ground)
Flow Rate (Litre/Minute)	Frequency (Hz)/7.5
Measurement Error	$\pm$5%

Table 3. Characteristic of Flow-meter

Volt (core) voltage regulators, 3 LEDs, 1 pushbutton switch. The core chip of this module, Altera Cyclone II, EP2C5T144C8N has 4068 logic elements, multiple 4k RAM blocks giving a total of 119,898 bits. Author configure the FPGA using Very High-Speed Hardware Description Langguage (VHDL) in Quartus II software.

The camera module, ESP32-Cam is a very competitive small-size minimum system with a footprint of only 27*40.5*4.5 mm and a deep sleep current of up to 6 mA. It has SPI flash 32 Mbit, 520 KB SRAM, 4 Mbit PSRAM, Bluetooth capability, 802.11 b/g/n WiFi capability, UART, SPI, I2C, PWM, 9 I/O port, on-board PCB antenna, gain 2 dBi, image format Grayscale, BMP, JPEG, 5 volt power supply range. The pixel size of image data

 doi:10.20944/preprints202205.0233.v1

PWM	Flowrate (LPM)
5000	3.3 ± 0.5
3000	2.7 ± 0.5
1000	1.3 ± 0.4

Table 4. Relation between PWM and volume flow rate

captured by ESP32-Cam is 160x120, with frame rate of 24 frame per second (FPS). Author create C++ code using Arduino IDE and embed it in to ESP32-Cam.

In PC/Laptop the author create python program to capture pixel data send by ESP32-Cam, and use it to create video data and place it in side specific folder. The folder and video name are specific base upon PWM data. Another python program is use to create 10 second video from original video. The original and 10 second videos can be found in author github page which the link can be found in supplementary section of this paper. It is already organize in specific folder base on the PWM values.

5. Results

5.1. Temporal Binary Pattern Image

Using MOCWFS we have 15106 video data set which reader can found in our github link, we also create youtube channel, so reader can see the how MOCWFS work. The web address of our github repository and YouTube channel are given in Data Availability Section. The data set are divided in to 4 folder which correlated with PWM value given to water pump. Using flow-meter installed after water pump, we able to estimate the volume flow rate generated by the pump. Table 4 show relation between PWM with estimated flow rate. Unfortunately due to limitation of the flow-meter, when PWM value of 500 the flow rate reading is 0. Although in PWM 500 water is still moving. The reader can see the water movement when PWM is 500 in our github link.

5.2. Temporal Binary Pattern Image

Figure 14 show various pattern produced by TBPI on various PWM value. We can see on the lower PWM value, there is a lot of black pixels appear. As the PWM value goes high, or volume flow-rate is increasing, this black pixels is decreasing. At PWM value of 3000 and 5000 the pattern is almost similar.

5.3. Histogram of Temporal Binary Pattern

A comparable phenomenon is seen on the histogram of the TBPI as we can see in Fig.15. The resulting histogram shows the difference between low and high value PWM. The higher the PWM value, the histogram will resemble a box. At the PWM 3000 and 5000 the histograms produced by both values are almost the same.

5.4. Feed Forward Neural Network Training

From 15106 video data set, we divide the data to 10574 data for training and 4532 for testing. We train histogram data using Google Colabs and achieved accuracy is between 72 to 73 %, the training time around 10 to 16 minute. Fig.16 show accuracy during training process.

6. Discussion

As described in previous sections, TBP is able to extract temporal feature of WSV. We can visually see how TBPI are differ between pump PWM value. Except for PWM value of 5000 and 3000 where TBPI have simmilar pattern. Histogram of TBPI (TBPIH) also show significant difference between PWM value 500 and the rest of the value, but not for PWM value 3000 and 5000 where TBPIH are almost similar. The similarity of TBPI and TBPIH of

Preprints (www.preprints.org) | NOT PEER-REVIEWED | Posted: 17 May 2022 doi:10.20944/preprints202205.0233.v1

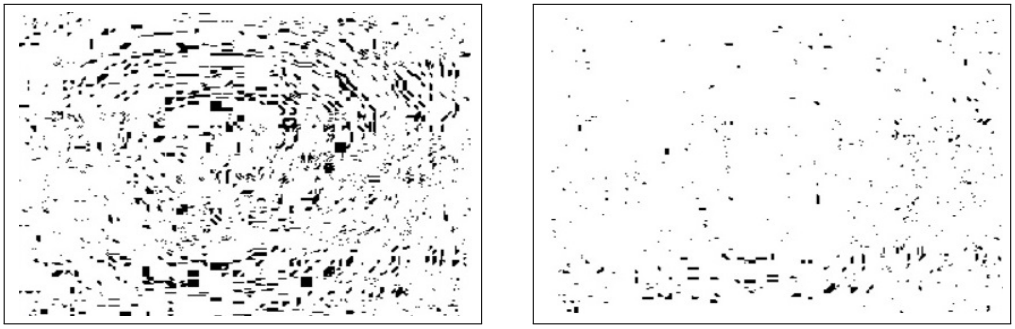

(a) $s(x, y, t)$ when PWM value 500 **(b)** $s(x, y, t)$ when PWM value 1000

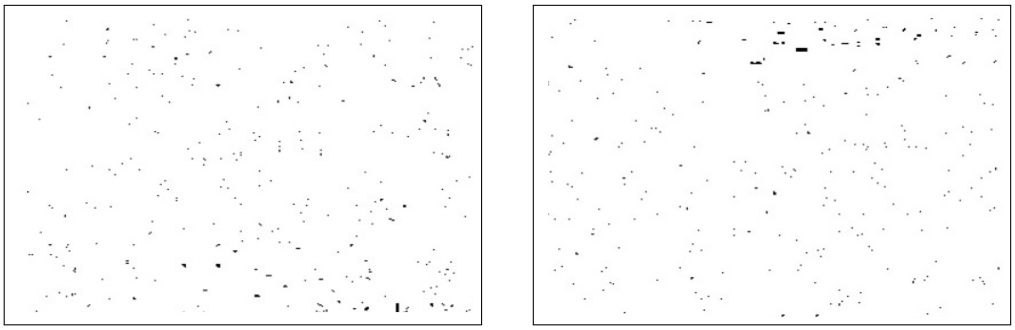

(c) $s(x, y, t)$ when PWM value 3000 **(d)** $s(x, y, t)$ when PWM value 5000

Figure 14. TBP Transformation on various PWM value

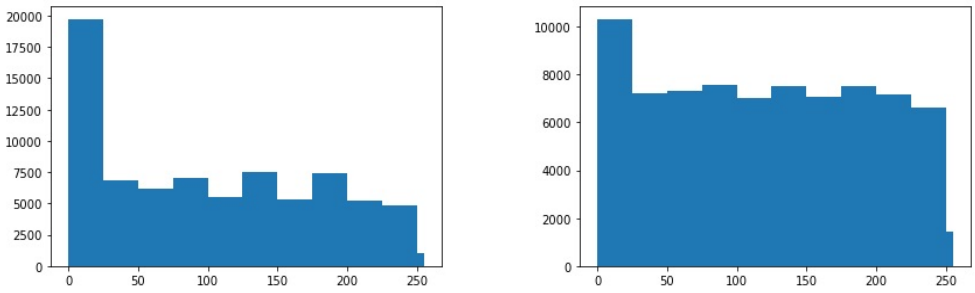

(a) Histogram of $s(x, y, t)$ when PWM value 500 **(b)** Histogram of $s(x, y, t)$ when PWM value 1000

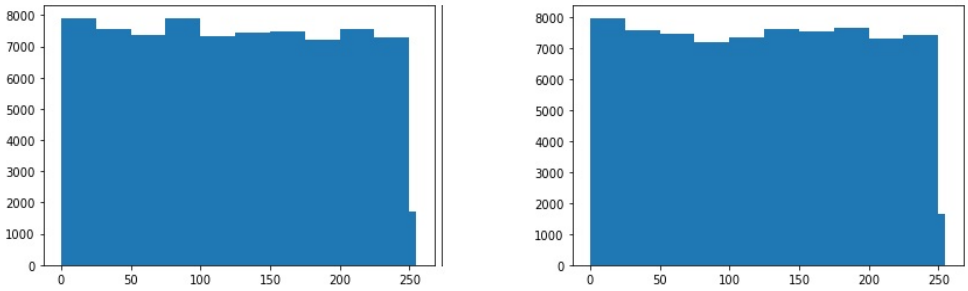

(c) Histogram of $s(x, y, t)$ when PWM value 3000 **(d)** Histogram of $s(x, y, t)$ when PWM value 5000

Figure 15. Histogram of TBP Transformation on various PWM value

these two PWM values may be due to the similar maximum changes in water ripple height. The water thrust generated by the pump between PWM 3000 and 5000 cannot produce a water ripple height that can be significantly distinguished by the TBP method. But in low PWM value or low flow rate, such as PWM 500 and PWM 1000, TBP method are able to distinguish them significantly.

Preprints (www.preprints.org) | NOT PEER-REVIEWED | Posted: 17 May 2022 doi:10.20944/preprints202205.0233.v1

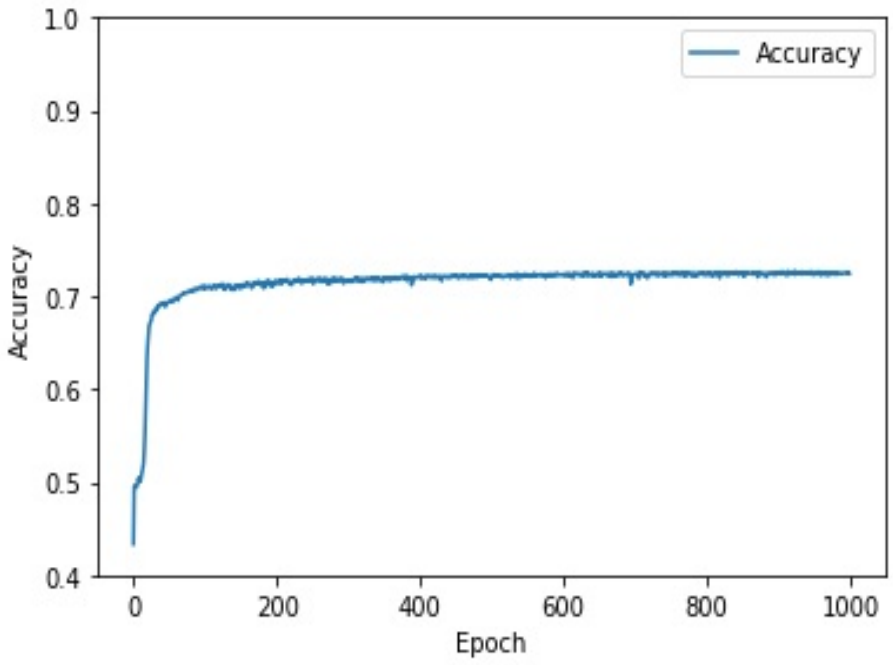

Figure 16. Accuracy of FNN Training

At the low flow rate, PWM 500, black pixel dominate the region. We can see this at Histogram of TBIP at Fig. 15a, where black pixels (integer value of 0) reach 20000 count.In binary form black pixel is equal to 00000000. This is mean many of pixels in the area do not vary a lot. When PWM value is increase to 10000, the flow is also increase, black pixels is decreasing as we can see in 15b. The black pixels value is 10000, and other pixels value is increasing compare to Fig 15a. When th PWM value reach 3000 and 5000, in Fig 15c and Fig 15d, the black pixels count is 8000, while other pixels value is in the range between 7000-8000 except pixels value of 250 which is only 2000. The disability to distinguish WSV in higher PWM pump may caused by bit size in TBPI. Since it is only 8 bits, pixel variations due to the movement of water in high flow rates may not be captured. More bit size required, which means more frames to be captured.

Although TBPIH is unable to distinguish variation of water ripple in high flow rate. Training result using FNN show quite fair results with more than 70% of accuracy. At first author use RSME as loss function, and the accuracy of training is around 50%, and 5 layers were used. When Loss Function are changed to MAE, the training accuracy is increased, and only 2 layers are required. As known the difference between RSME and MAE is on how it handle out layer data. RSME is more prone to out layer data, while MAE are more robust. So MAE is more appropriate to handle TBPIH data, since it may contain out layer. Although MAE had increase training accuracy, but since at high PWM value or flow rate TBP unable to distinguish them appropriately, maximum accuracy that can be achieved is 73%.

With this accuracy, TPBIHNN can be an alternative method for WSV estimation using camera. Since it use XOR operation to extract temporal pattern this method has low computation complexity and can be implemented in micro controller or FPGA. The greatest computational complexity mostly comes from FNN which has 14,983 parameters that must be calculated to predict the results. Compare to STIV which need 2D-Fourier Transform, TBPIH is have less time complexity. In term of memory, since TBPIH result is the same size as original image, compared to VLBP or VLBC or LBP-TOP the proposed method have less memory requirement.

7. Conclusion

This study had shown that temporal feature of WSV can be extracted using XOR operator. The proposed method TBPIHNN has fair accuracy of 73%, it's still had draw back when distinguish WSV at medium flow rate (2.7 to 3.3 LPM). Further work should be carried out to improve TBPIHNN by increasing bit size in TBPI, or using more light Neural Network structure such as Extreme Learning Machine to reduce network parameter.

Author Contributions: B.H.S., Conceptualization, Data curation, Formal analysis, Investigation, Methodology, Software, Resources, Writing—original draft; P.M., Conceptualization, Methodology, Validation, Resources, Funding acquisition, Project administration, Supervision; S.W., Conceptualization, Methodology, Validation, Resources, Supervision, Writing - review editing. All authors have read and agreed to the published version of the manuscript.

Funding: This work was supported by funding from University Grant for Internationally Indexed Publication of Students' Final Project (Hibah PUTI Doctor) Contract No: NKB563/UN2.RST/HKP.05.00 administered by the Directorate of Research and Community Engagement (DRPM), Universitas Indonesia.

Data Availability Statement: Open channel water flow dataset which is use in this paper is avaliable in the following Github Link https://github.com/BenSirenden/Mini-Open-Channel-Water-Flow-Simulator. The reader can watch how MOCWFS work in the following youtube link https://www.youtube.com/watch?v=1MUPqTsU1X4&t=2s.

Acknowledgments: The authors would like to thanks "Degree By Research" Scholarship Program of Indonesia National Research and Innovation Agency (BRIN) for the support. .

Conflicts of Interest: The authors declare no conflict of interest.

References

1. Rozos, E.; Dimitriadis, P.; Mazi, K.; Lykoudis, S.; Koussis, A. On the Uncertainty of the Image Velocimetry Method Parameters. *Hydrology* **2020**, *7*. doi:10.3390/hydrology7030065.
2. Gleason, C.J.; Durand, M.T. Remote Sensing of River Discharge: A Review and a Framing for the Discipline. *Remote Sensing* **2020**, *12*. doi:10.3390/rs12071107.
3. Livoroi, A.H.; Conti, A.; Foianesi, L.; Tosi, F.; Aleotti, F.; Poggi, M.; Tauro, F.; Toth, E.; Grimaldi, S.; Mattoccia, S. On the Deployment of Out-of-the-Box Embedded Devices for Self-Powered River Surface Flow Velocity Monitoring at the Edge. *Applied Sciences* **2021**, *11*. doi:10.3390/app11157027.
4. Trieu, H.; Bergström, P.; Sjödahl, M.; Hellström, J.G.I.; Andreasson, P.; Lycksam, H. Photogrammetry for Free Surface Flow Velocity Measurement: From Laboratory to Field Measurements. *Water* **2021**, *13*. doi:10.3390/w13121675.
5. Fulton, J.W.; Mason, C.A.; Eggleston, J.R.; Nicotra, M.J.; Chiu, C.L.; Henneberg, M.F.; Best, H.R.; Cederberg, J.R.; Holnbeck, S.R.; Lotspeich, R.R.; et al. Near-Field Remote Sensing of Surface Velocity and River Discharge Using Radars and the Probability Concept at 10 U.S. Geological Survey Streamgages. *Remote Sensing* **2020**, *12*. doi:10.3390/rs12081296.
6. Naves, J.; García, J.T.; Puertas, J.; Anta, J. Assessing different imaging velocimetry techniques to measure shallow runoff velocities during rain events using an urban drainage physical model. *Hydrology and Earth System Sciences* **2021**, *25*, 885–900. doi:10.5194/hess-25-885-2021.
7. Eltner, A.; Mader, D.; Szopos, N.; Nagy, B.; Grundmann, J.; Bertalan, L. USING THERMAL AND RGB UAV IMAGERY TO MEASURE SURFACE FLOW VELOCITIES OF RIVERS. *The International Archives of the Photogrammetry, Remote Sensing and Spatial Information Sciences* **2021**, *XLIII-B2-2021*, 717–722. doi:10.5194/isprs-archives-XLIII-B2-2021-717-2021.
8. Wu, H.; Zhao, R.; Gan, X.; Ma, X. Measuring Surface Velocity of Water Flow by Dense Optical Flow Method. *Water* **2019**, *11*. doi:10.3390/w11112320.
9. Genç, O.; Ardıçlıoğlu, M.; Ağıralioğlu, N. Calculation of mean velocity and discharge using water surface velocity in small streams. *Flow Measurement and Instrumentation* **2015**, *41*, 115–120. doi:https://doi.org/10.1016/j.flowmeasinst.2014.10.013.
10. Fujita, I.; Watanabe, H.; Tsubaki, R. Development of a non-intrusive and efficient flow monitoring technique: The space-time image velocimetry (STIV). *International Journal of River Basin Management* **2007**, *5*, 105–114, [https://doi.org/10.1080/15715124.2007.963531(doi:10.1080/15715124.2007.9635310.
11. Fujita, I. Discharge Measurements of Snowmelt Flood by Space-Time Image Velocimetry during the Night Using Far-Infrared Camera. *Water* **2017**, *9*. doi:10.3390/w9040269.
12. Fujita, I.; Notoya, Y.; Tani, K.; Tateguchi, S. Efficient and accurate estimation of water surface velocity in STIV. *Environmental Fluid Mechanics* **2019**, *19*, 1363–1378. doi:10.1007/s10652-018-9651-3.
13. Tsubaki, R. On the Texture Angle Detection Used in Space-Time Image Velocimetry (STIV). *Water Resources Research* **2017**, *53*, 10908–10914, [https://agupubs.onlinelibrary.wiley.com/doi/pdf/10.1002/2017WR021913]. doi:https://doi.org/10.1002/2017WR021913.

14. Tsuji, Issei.; Tani, Kojiro.; Fujita, Ichiro.; Notoya, Yuichi. Development of Aerial Space Time Volume Velocimetry for Measuring Surface Velocity Vector Distribution from UAV. *E3S Web Conf.* **2018**, *40*, 06011. doi:10.1051/e3sconf/20184006011.
15. Watanabe, K.; Fujita, I.; Iguchi, M.; Hasegawa, M. Improving Accuracy and Robustness of Space-Time Image Velocimetry (STIV) with Deep Learning. *Water* **2021**, *13*. doi:10.3390/w13152079.
16. Han, X.; Chen, K.; Zhong, Q.; Chen, Q.; Wang, F.; Li, D. Two-Dimensional Space-Time Image Velocimetry for Surface Flow Field of Mountain Rivers Based on UAV Video. *Frontiers in Earth Science* **2021**, *9*. doi:10.3389/feart.2021.686636.
17. Strelnikova, D.; Paulus, G.; Käfer, S.; Anders, K.H.; Mayr, P.; Mader, H.; Scherling, U.; Schneeberger, R. Drone-Based Optical Measurements of Heterogeneous Surface Velocity Fields around Fish Passages at Hydropower Dams. *Remote Sensing* **2020**, *12*. doi:10.3390/rs12030384.
18. Rojas Arques, S.; Rubinato, M.; Nichols, A.; Shucksmith, J.D. Cost effective measuring technique to simultaneously quantify 2D velocity fields and depth-averaged solute concentrations in shallow water flows. *Flow Measurement and Instrumentation* **2018**, *64*, 213–223. doi:https://doi.org/10.1016/j.flowmeasinst.2018.10.022.
19. Tauro, F.; Tosi, F.; Mattoccia, S.; Toth, E.; Piscopia, R.; Grimaldi, S. Optical Tracking Velocimetry (OTV): Leveraging Optical Flow and Trajectory-Based Filtering for Surface Streamflow Observations. *Remote Sensing* **2018**, *10*. doi:10.3390/rs10122010.
20. Pearce, S.; Ljubičić, R.; Peña-Haro, S.; Perks, M.; Tauro, F.; Pizarro, A.; Dal Sasso, S.F.; Strelnikova, D.; Grimaldi, S.; Maddock, I.; et al. An Evaluation of Image Velocimetry Techniques under Low Flow Conditions and High Seeding Densities Using Unmanned Aerial Systems. *Remote Sensing* **2020**, *12*. doi:10.3390/rs12020232.
21. Legleiter, C.J.; Kinzel, P.J. Inferring surface flow velocities in sediment-laden Alaskan rivers from optical image sequences acquired from a helicopter. *Remote Sensing* **2020**, *12*. doi:10.3390/rs12081282.
22. Zhao, H.; Chen, H.; Liu, B.; Liu, W.; Xu, C.Y.; Guo, S.; Wang, J. An improvement of the Space-Time Image Velocimetry combined with a new denoising method for estimating river discharge. *Flow Measurement and Instrumentation* **2021**, *77*, 101864. doi:https://doi.org/10.1016/j.flowmeasinst.2020.101864.
23. Sirenden, B.; Mursanto, P.; Wijonarko, S. Dynamic Texture Analysis Using Auto-correlation Function of Histogram Similarity Measure from Galois-Field Texture Representation of Water Flow Video. Proceeding - 2020 International Conference on Radar, Antenna, Microwave, Electronics and Telecommunications, ICRAMET 2020; Institute of Electrical and Electronics Engineers Inc.: United States, 2020; pp. 51–56. doi:10.1109/ICRAMET51080.2020.9298601.
24. Bernd, J.; Haussecker, H.; Geißler, P. *Handbook of Computer Vision and Applications*; Vol. 2, Academic Press, 1999.
25. Ma, Y.; Cisar, P. Event detection using local binary pattern based dynamic textures. 2009 IEEE Computer Society Conference on Computer Vision and Pattern Recognition Workshops, 2009, pp. 38–44. doi:10.1109/CVPRW.2009.5204204.
26. Juefei-Xu, F.; Boddeti, V.; Savvides, M. Local Binary Convolutional Neural Networks. 2017 IEEE Conference on Computer Vision and Pattern Recognition (CVPR); IEEE Computer Society: Los Alamitos, CA, USA, 2017; pp. 4284–4293. doi:10.1109/CVPR.2017.456.
27. Zhao, X.; Lin, Y.; Heikkilä, J. Dynamic Texture Recognition Using Volume Local Binary Count Patterns With an Application to 2D Face Spoofing Detection. *IEEE Transactions on Multimedia* **2018**, *20*, 552–566. doi:10.1109/TMM.2017.2750415.
28. Sima, J.; Dong, Y.; Wang, T.; Zheng, L.; Pu, J. Extended Contrast Local Binary Pattern for Texture Classification. *International Journal of New Technology and Research* **2018**, *4*.
29. Wei, X.; Yu, X.; Liu, B.; Zhi, L. Convolutional neural networks and local binary patterns for hyperspectral image classification. *European Journal of Remote Sensing* **2019**, *52*, 448–462, [https://doi.org/10.1080/22797254.2019.1634980]. doi:10.1080/22797254.2019.1634980.
30. Shivashankar, S.; Kudari, M.; Hiremath, P.S. Galois Field-based Approach for Rotation and Scale Invariant Texture Classification. *International Journal of Image, Graphics and Signal Processing* **2018**, *10*, 56–64. doi:10.5815/ijigsp.2018.09.07.
31. Shivashankar, S.; Kudari, M.; Hiremath, P.S. A Galois Field based Texture Representation for Face Recognition. *International Journal of Applied Engineering Research* **2018**, *13*, 13460–13465.
32. Paygude, S.; Vyas, V.; Khadilkar, C. Velocity and Orientation Detection of Dynamic Textures Using Integrated Algorithm. *International Journal of Image, Graphics and Signal Processing (IJIGSP)* **2018**, *10*, 39–46. doi:10.5815/ijigsp.2018.12.05.
33. Hodges, B.R. Conservative finite-volume forms of the Saint-Venant equations for hydrology and urban drainage. *Hydrology and Earth System Sciences* **2019**, *23*, 1281–1304. doi:10.5194/hess-23-1281-2019.